UK Atomic Energy Authority

UKAEA-STEP-PR(25)26

Thomas Wilson, Mark Henderson, Hana El-Haroun,
Anurag Saigiridhari

Heating and Current Drive in STEP: Neutral Beam Injection

Heating and Current Drive in STEP: Neutral Beam Injection

Thomas Wilson, Mark Henderson, Hana El-Haroun, Anurag Saigiridhari

This is a preprint of a paper submitted for publication in Nuclear Fusion

Heating and Current Drive in STEP: Why Neutral Beam Injection is not desirable

Thomas Wilson, Mark Henderson, Hana El-Haroun, Anurag Saigiridhari, Emmi Tholerus

Abstract

STEP [1] (Spherical Tokamak for Energy Production) is the UK's prototype fusion power plant programme aiming to demonstrate net electrical output from a spherical tokamak. The plasma scenarios require completely non-inductive current drive for the flat-top and the majority of the ramp-up/down phases [2]. Most of the current ($\sim 80\%$) is self-generated by the plasma pressure gradient with the remainder provided by the heating and current drive (HCD) system. The capabilities and limitations of Neutral Beam Injection (NBI) for current drive in relevant STEP scenarios are presented, as well as the additional integration, technology readiness level, maintainability, and financial considerations that determine the optimal HCD system for a reactor class tokamak. It is demonstrated that, in isolation, NBI has excellent current drive efficiency achieving $\zeta = 0.4$ at $\rho = 0$ rising to $\zeta = 1.4$ at $\rho = 0.8$ for beam energies $\leq 1\mathrm{MeV}$. However, once considered in an integrated design, the poor wall-plug efficiency, large size and consequent high cost makes NBI undesirable in STEP compared to microwave based HCD.

1 Introduction

STEP [1] (Spherical Tokamak for Energy Production) is the UK's prototype fusion power plant programme, currently in the design phase with the aim to demonstrate net electrical output from a spherical tokamak (ST) fusion reactor by the 2040s. STs can operate at higher β_N compared to conventional aspect ratio devices and achieve higher elongation κ. As fusion power $P_{Fus} \propto \beta_N^4 B^4 \kappa^5 R_{geo}^3 / A^3$ [2] the ST could offer a pathway to compact low magnetic field B devices with the same fusion power but potentially reduced cost compared to conventional tokamaks.

STEP is designed to be a steady state device with fully non-inductive current drive during the plasma current I_p flat-top phase and a majority of the ramp-up and ramp-down with no reliance on a central solenoid. A large fraction ($\sim$80%) is self-generated via the plasma pressure gradient, the bootstrap current [3], with the remainder provided the by heating and current drive (HCD) system(s). Any solenoid will be small to maintain a low aspect ratio device, so the HCD system must be able to actuate over a majority of the plasma cross section throughout the plasma discharge (ramp-up, flat-top, ramp-down) to achieve the targeted current profile.

In order to achieve net electric output, the optimum HCD system should drive a maximum current with the least power taken from the national electrical grid. There are multiple HCD systems that can drive current as required for STEP, these include:

- Microwave based HCD: electron cyclotron (EC), electron Bernstein wave (EBW)
- Radio wave based HCD: lower hybrid (LH), helicon wave (HW)
- Neutral beam injection (NBI)

This paper aims at assessing the capabilities and limitations of the NBI system in relevant STEP scenarios, in addition to the integration, technology readiness level, maintainability, and financial considerations that determine the optimum HCD mix for STEP.

These requirements for an optimum HCD system on STEP are defined in Section 2. Section 3 introduces NBI and defines the required data to assess it based on the defined criteria for STEP. The modelling methodology using the NBI codes PENCIL [4] and ASCOT [5] is described in Section 4, followed by the

modelled results for the flat-top and ramp-up in Section 5. A discussion of pertinent engineering issues integrating NBI into STEP is presented in Section 6. A summary of the NBI's compatibility with targeted objectives is provided in Section 7.

2 Assessment Criteria for a STEP HCD System Capabilities

The critical parameter determining the STEP HCD system was the efficiency of the driven current relative to the power taken from the grid, the product of the plug-to-plasma efficiency and the current drive efficiency. In particular, during the flat top phase the HCD system is the largest parasitic load to generating net electrical power back to the grid. The total HCD system efficiency is therefore an important contribution to the required fusion gain factor $Q = P_{Fus}/P_{HCD}$ unless Q is much larger than the $Q \approx 11$ targeted for STEP. However, the STEP HCD mix also considered the technological requirements, system integration and life-cycle cost. We will take inspiration from to previous HCD studies for ITER [6] and DEMO [7] but take a slightly different approach as unlike these machines STEP is to demonstrate fully non-inductive steady state operation.

The assessment criteria for the HCD system and an explanation of the methodology for these choices are introduced in the following paragraphs.

The assessment criteria were grouped into two main categories, first the 'physics' criteria:

- Availability in flat top and maximum current drive efficiency.
- Availability in ramp up and ramp down and maximum current drive efficiency.
- Availability for start up assist, both in breakdown and burn through.
- Flexibility to adjust deposition location for current profile control.

Followed by the 'engineering' criteria:

- Impact on vacuum vessel, magnets and blankets.
- Impact on tokamak building size.
- Total system cost.
- Technology readiness level of HCD system components on STEP timelines.
- Reliability, availability, maintainability and inspectability (RAMI).

The importance of the current drive efficiency has been described above. However, just driving the maximum current at a fixed location is insufficient, as the driven current profile must be tailored to match the missing current across the plasma cross section not supplied by the bootstrap to maintain an elevated safety factor profile $q > 2.3$ and achieve a broad current profile to improve vertical and resistive wall mode stabilisation. Therefore, the HCD system should be able to drive localised current across the entire plasma radius, ideally with narrow deposition, and be flexible to the changing current drive requirements across the plasma radius.

The HCD system is required during the ramp up and ramp down where there will be substantial variation in plasma density and temperature. The ability to drive current on axis is important during the ramp phases. Assistance in start-up to reduce or even remove the need of solenoid driven current is also desirable.

It is possible some traditional functions required of HCD system on existing devices are not required for STEP. For example, it is possible pure electron heating plus α particle heating will be sufficient to maintain the ion temperature thus no ion heating would be required. It is also possible resistive wall modes can be controlled using passive or active system thus no torque injection is required. Keeping

$q > 2$ or ideally $q > 5/2$ would also remove the need for active control of low m/n Neoclassical Tearing Modes (NTMs). We will assume these statements to be true for the analysis in this paper.

While the physics requirements focused primarily on the current drive efficiency, the engineering criteria were more diverse and included factors not normally attributed to an HCD system. The HCD system must also fit into an integrated engineering design, synergising with the objectives of STEP such as net electrical power output (as stated above) but also avoid significant degradation to the self-sustaining tritium breeding i.e. avoiding large voids in the breeding blankets. The HCD system should minimise the port occupation and space around the tokamak to minimise impact to the tokamak and bio-shield volume.

The overall cost of the HCD system and its impact on costs to the tokamak and infrastructure must be minimised to keep fusion cheap enough to be economically viable. Hidden in the costs are the potential development costs on the STEP timeline to bring the technology readiness level to a sufficient maturity for reliable operation under the harsh conditions of the burning fusion environment.

Another crucial engineering criterion is the system Reliability, Availability, Maintainability and Inspectibility (RAMI). STEP aims at demonstrating a pathway toward industrialisation, which requires highly reliable systems in near continuous operation. In the event of a fault, the ability to detect and repair the fault with a minimal down time is crucial. Thus, an attempt is also made to quantify the complexity of maintenance and in-situ inspections of HCD components, particularly those inside nuclear safety boundaries where remote maintenance is required.

3 Neutral Beam Injection

Neutral Beam Injection (NBI) [8] is a traditional heating system on existing tokamaks, with high power NBI systems currently installed on a majority of existing tokamaks (for example JET, EAST, K-Star, DIII-D, MAST-U, ASDEX-U and LHD). A high power NBI system will also be installed on next generation devices such as ITER and JT60-SA. Neutral beam current drive (NBCD) has been experimentally measured in several tokamaks (JET [4], ASDEX [9] and MAST [10]). Furthermore, NBI has been modelled and optimised for ITER [6] and DEMO [7], primarily for core heating, but has also shown neutral beam current drive (NBCD) can be very efficient for the high energy beams ($\sim$1 MeV) considered.

NBI also has the benefits of providing ion heating, though the heating is primarily on electrons for when the beam energy is large. The rate of energy transfer to ions and electrons is equal when the beam energy E_b is equal to the critical energy W_{crit} while equipartition occurs when $E_b = 2.41W_{crit}$ [8]. For a deuterium beam injected into a 50/50 DT plasma $W_{crit} = 16.5T_e$ thus electron heating is dominant for $E_b > 39.8T_e$. Finally, NBI can inject torque into the plasma which induces rotation. This rotation can stabilise the resistive wall mode [2] and is predicted to help saturate electromagnetic turbulence in STEP [11].

As the size, density and effective charge of the target plasma increases, higher energy NBI sources are required to deposit power in the core. NBI systems can be categorised on whether they generate positive ions (PNBI) or negative ions (NNBI) ions in the source. PNBI is more technologically mature but have a maximum usable beam energy of $\approx 125\ \mathrm{keV}$ above which the neutralisation efficiency drops strongly causing the neutral power to decrease sharply. The JET NBI system is a good example of a high power PNBI system [12].

For higher energies negative ion systems are required. The maximum theoretical neutralisation efficiency of NNBI is 58% and is independent of beam energy. However, high current NNBI sources are

less technologically mature above $500\ \mathrm{keV}$. JT60-SA is the highest energy NBI source injected into a tokamak, designed for a maximum beam energy of $500\ \mathrm{keV}$ [13]. The LHD NNBI system has demonstrated relatively long pulse NNBI operation of up to 2 mins though at very low power [14]. ITER are developing a $1\mathrm{MeV}$ NNBI system [15] while an energy of $1.5\mathrm{MeV}$ was considered the maximum extrapolation above the ITER design on DEMO timelines [16]. We only consider energies $\leq 1\mathrm{MeV}$ as the cost and development time for higher energy NBI sources is considered prohibitive and too risky for the fast time scales targeted for STEP.

Based on the criteria discussed in the previous section, the following aims were set for the assessment of NBI in STEP

a) In the flat top, find the envelope of maximum current drive efficiency and the associated NBI parameters at each radial location in the plasma as a function of beam energy. The NBI parameters must satisfy the machine constraints e.g. wall power loadings.
b) Find the minimum density in the ramp up required to use NBI at each radial location in the plasma as a function of beam energy while satisfying machine constraints.
c) Generate a low fidelity CAD model to find the restrictions on NBI injection parameters from the integrated design.
d) Dimension the required beam energy and power of an NBI system in STEP and assess the 'engineering' criteria of this dimensioned system.

The 'machine constraints' are the restrictions placed on the NBI system by being part of an integrated reactor design. One example is that the availability of NBI in any phase can be limited if the stray power striking the vessel wall exceeds the thermal limits of impacted components, primarily due to shinethrough (non-ionised neutral power incident on the wall). Another example is the limitations in injection trajectories due to the finite size of the beamline fitting into a port plug angling between the poloidal and toroidal field coils. These later limitations were used to develop a simplified NBI injector model used to cover the allowable injection trajectories, scanning over a wide range of beam energies.

The NBI codes PENCIL and ASCOT, coupled to the JINTRAC/JETTO modelling suite [17], were used to calculate the NBI heating, current drive, shinethrough and first orbit losses. We scan in beam energy, source height and both the poloidal and toroidal injection angles to generate a dataset of driven current, shinethrough and first orbit losses used to evaluate a) and b) above.

With the results and the restrictions from the CAD model, the optimum parameters best meeting the 'physics' criteria can be determined, which includes optimum beam energy and power yielding the best current drive performance. Defining the NBI parameters then leads to a refinement of the CAD model based on existing NBI systems to assess the 'engineering' criteria and give a final assessment of NBI in STEP.

4 Methodology

4.1 Flat Top Operating Point

The HCD mix assessment was performed in parallel with determining the optimum plasma parameters and physical dimensions of the STEP device. Each HCD system was assessed for performance in an 'optimal' plasma operating point with a radius, magnetic field and density chosen for peak performance of the specific HCD system e.g. the ECCD plasma had high field, low density to avoid cut-off, the NBI plasma was compact with a weak field to favour lower acceleration voltages, etc. It was also hoped a small weak field machine would also keep STEP costs to a minimum. An advantage of NBI compared to electromagnetic wave based HCD is its operation does not depend explicitly on magnetic field strength, which places less constraints on the design.

All of these plasma operating points were created using the 1.5D core transport solver JETTO [17] based on output from the power plant optimisation code PROCESS [18]. All operating points had $Q > 10$ and approximately 100MW of auxiliary heating power. Details on the NBI operating point are given in Table 1 and Figure 1. A tokamak CAD model was then scaled down to the correct size from a larger pre-concept test operating point for ECCD.

The magnetic equilibrium was generated using the fixed boundary Grad-Shafranov solver ESCO [17] with a D-shaped separatrix model [19] and evolved self consistently with the kinetic profiles to steady state. The equilibrium is up-down symmetric and contains no X points. Heat and particle transport have a neoclassical component computed by NCLASS supplemented with anomalous heat diffusivity calculated with the semi-empirical Bohm/gyro-Bohm model. Full details of the transport model can be found here [20]. The ion and electron temperatures are assumed equal. There is no rotation and Zeff is flat 1.8 with only He and Xe impurities.

There are significant simplifications used in generating this plasma operating point but it is only meant to be a target plasma for evaluation of NBCD in STEP relevant parameter regimes. A more mature operating point developed after this analysis is described in these references [1][2].

Table 1: Parameters of the scaled down STEP model used for the NBCD optimisation study.

Major Radius [m]	2.5	Minor Radius [m]	1.5
Elongation	2.8	Triangularity	0.5
Magnetic Field at geometric axis [T]	2.4	Plasma Current [MA]	16.5
$\langle n_e \rangle$ $[10^{19}\mathrm{m}^{-3}]$	18.9	<Te> [keV]	8.3
Zeff	1.8 (He/Xe Impurity)	Fusion Power [GW]	1
Greenwald Fraction [%]	80	Bootstrap Fraction [%]	75

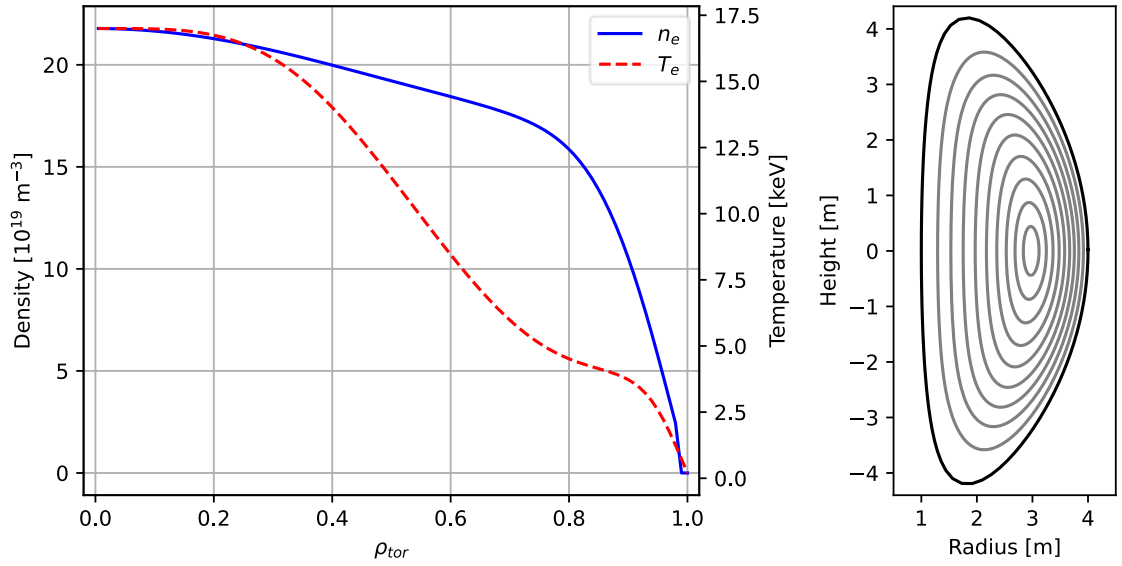

Figure 1: Electron density (solid) and temperature (dashed) profiles vs root normalised toroidal flux ρ_{tor} (left) and contours of root normalised poloidal flux (right) for STEP NBI operating point.

4.2 PENCIL and ASCOT

The heating, current drive, shinethrough and first orbit losses are estimated using the PENCIL and ASCOT NBI codes coupled to the JETTO/JINTRAC integrated modelling suite. All kinetic profiles were 'frozen' and not modified by the injected beam. An initial large parameter scan of the NBCD was performed using PENCIL, which is well suited as large parameter scans take only a few seconds on a single CPU while a single ASCOT run takes several hours parallelised over multiple CPUs.

The PENCIL code [4] has two parts: a beam deposition calculation using ADAS [21] cross sections and a Fokker-Planck solver to calculate the fast ion distribution. The beam is broken down into an array of parallel non-divergent beamlets each of which carries a fraction of the total particles and power in a 2D Gaussian distribution across the beam cross section. Analytic approximations for plasma equilibrium are used to increase the calculation speed. As a result, PENCIL does not exactly describe the magnetic field pitch angle and therefore cannot correctly calculate the current drive. The beam deposition and shinethrough are reliably calculated, as demonstrated in previous benchmarks against ASCOT and NUBEAM [22] and our own comparisons.

Whilst the inaccuracies in PENCIL due to the physics approximations mean the results cannot be used directly, it is used to rapidly narrow the parameter range which can then be investigated using the more sophisticated ASCOT code. This makes the computational expense of the full HCD assessment tractable while still thoroughly exploring the full parameter space.

ASCOT is a Monte Carlo code which solves the kinetic equation of beam ions in a plasma [5]. It has a full description of the magnetic field and so describes pitch angle effects, a realistic beamlet model with dispersion and models finite orbit effects such as first orbit losses. A guiding centre version of ASCOT is used for reduced computation time as it had little effect on the calculated current drive. Each run used 10,000 markers and was run for 0.5 seconds updating the fast ion distribution every 25ms. Final quantities were averaged over 0.2-0.5s. No other fast ion losses like charge exchange and toroidal ripple are considered.

The beam driven current in ASCOT is calculated from the parallel velocity moment of the fast ion distribution multiplied by an electron shielding factor from Mikkelsen and Singer [23], who reference a form given by Start and Cordey [24]. This version of the shielding factor is valid for arbitrary aspect ratio and is thus applicable to STs like STEP.

All values of current drive are normalised to injected NBI power i.e., a current drive efficiency is assumed independent of the injected power. Beam power quoted is the neutral power incident on the plasma. Transmission losses like re-ionisation are not calculated as the duct and beamline are not modelled. Current drive efficiency is quoted both as a raw efficiency $I_{NB}[\mathrm{kA}]/P_{NB}[\mathrm{MW}]$ and a normalised efficiency [25]:

$$\zeta = 32.7\frac{n_e[10^{20}m^{-3}]R_{mag}[m]I_{NB}[\mathrm{MA}]}{T_e[\mathrm{keV}]P_{NB}[\mathrm{MW}]}$$

The term $\sim n_e/T_e$ comes from normalising via a characteristic rate at which currents are dissipated in the plasma via collisions. The term $\sim R_{mag}$ is approximately the ratio of the flux surface area to the flux tube volume which accounts for the fact power is smeared over the flux tube volume but current can only be driven through the cross-sectional area. Physical constants are gathered to give the pre-factor 32.7.

ζ is the adopted metric to compare current drive efficiency for each HCD system in its 'optimal' plasma. Note that ζ can not be used to map the achievable current drive for a given NBI system onto a different plasma or machine size as this would require an adjustment in acceleration energy and trajectory.

5 NBI Parameter Scans

The neutral beam injection parameters that can be varied for optimising ζ are maximum beam energy E_b and the injection trajectory, defined by the tangency point (R_T, Z_T) and source location (R_S, Z_S). These trajectory parameters can be related to the toroidal steering angle α ($\alpha > 0$ = counter-clockwise) and poloidal steering angle β ($\beta > 0$ = downwards) via the formulas

$$\sin\alpha = \frac{R_T}{R_S} \quad \tan\beta = \frac{Z_S - Z_T}{\sqrt{R_S^2 - R_T^2}}$$

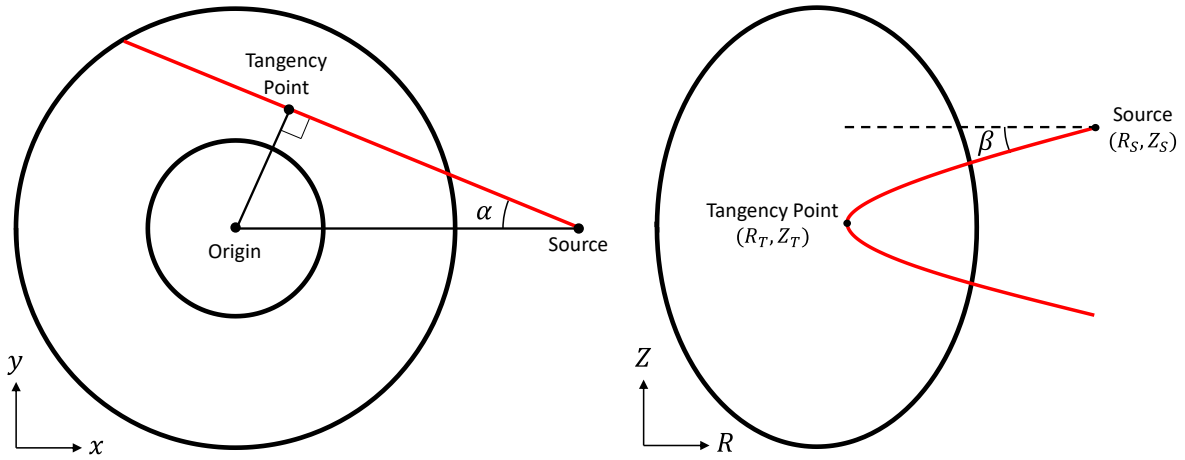

Figure 2: Diagram of the parameters defining the NB injection trajectory, projected into the $x-y$ plane (left) and a poloidal slice (right).

The maximum beam energy E_{beam} defines the maximum acceleration energy achievable by the injector. Note the injector can be designed to work at lower energies but consequently lower power. The beam focus was set at the tangency point. Fisch gives an estimate that NBCD peaks for $E_b = 40A_bT_e$ [26], where A_b is the beam ion atomic mass, thus we use deuterium beams instead of tritium to minimise the required beam energy. Note in a power plant the NBI would have to be 50/50 D-T to maintain the core isotope ratios.

Changing the injection parameters alters the density, energy and pitch angle of fast ions deposited on each flux surface which changes the beam driven current. Here, the PENCIL runs were instrumental in performing the large parameter scans over the injection parameters to identify regions of parameter space with high current drive efficiency below the shinethrough limit. Then a refined scan was performed in ASCOT to calculate accurate current drive values and first orbit losses.

A limit of wall loading of $0.5\ \mathrm{MW}/m^2$ is assumed, the same as suggested for ITER. Note that this limit could be increased to $4\ \mathrm{MW}/m^2$ using wall armour as was considered for ITER [27], though this would degrade the tritium breeding. Values for shinethrough stated assume a steady state beam. It is possible to modulate the beam to reduce the shinethrough and allow use at lower densities, for example during the ramp-up/down phases. However, this results in only a minor extension in the minimum NBI operating density which is considered insignificant.

Table 2: Parameters of the neutral beam injectors for JET [12]*, JT-60SA* [28] *and ITER* [15].

System	Beam Energy [keV]	Maximum Power [MW]	Width / Height [m]	Ion Type	Divergence [mrad]
JET	125	2.2	0.5 / 0.2	Positive	12.2
JT-60SA	500	10	0.45 / 1.1 (5 segments)	Negative	5
ITER	1000	16.5	1.6 / 0.8 (4 segments)	Negative	3 (plus halo at 30)

Despite the fact these injectors all have different sizes and maximum power, all have a similar average power density of $\sim 20\ \mathrm{MW\,m^{-2}}$. A simplification in the beam profile was assumed, using a $5\ \mathrm{MW}$ circular gaussian beam of 0.3m radius with e-folding length equal to the radius. In power terms this corresponds to 2 JET injectors, half a JT60-SA injector or a quarter of the ITER injector. This neglects beam shape effects, which are taken as second order effects on current drive efficiency as compared to injection energy and launch trajectory. This is an idealised model but a similar process was applied to equivalent assessments of the other HCD systems to minimise time and simplify analysis of the parametric scans.

This injector model has a peak power density equal to the maximum shinethrough power density at $0.14\mathrm{MW}$ total power, i.e. $\sim 1\%$ total power for $10\ \mathrm{MW}$ injected, the maximum possible power that can be fitted to a single port. This is a viable estimate as the STEP model test injector has the same power density as the existing injectors of Table 2 over similar ranges in acceleration voltages.

A 1% total power limit is also assumed for first orbit losses. This is a crude approximation as first orbit losses generate areas of high-power density on the wall due to the way ions are lost but a more accurate calculation is beyond the scope of this paper.

5.1 Flat Top

An initial scan was performed in PENCIL scanning injection energy E_b from 100 to 1000 keV in 100 keV steps, source height Z_s from 0 to 4m in 0.15m steps and tangency radius R_T from 1.5 to 4m in 0.15m steps. The source radius R_s was set at 6m and the tangency height Z_T was set equal to Z_s. For each injection energy, the scan points were binned using the root normalised toroidal flux ρ_{tor} of the peak in the driven current profile with bin width $\rho_{tor} = 0.05$. Simulations with shinethrough $> 1\%$ were discarded. In each bin, the simulation with highest raw current drive efficiency η was obtained to define the maximum current driven efficiency as a function of ρ_{tor}. The normalised current drive efficiency ζ was calculated using the density and temperature values at the bin centre. These profiles are shown in Figure 3 coloured by injection energy.

The PENCIL scan indicated injection energies below 300 keV are insufficient to penetrate the pedestal region. Thus, the use of positive ion injectors is ruled out even for the smallest of STEP device choice options, as the primary role of the HCD system is to drive current for $\rho_{tor} \leq 0.8$. Injection energies of 1000 keV were able to achieve core deposition. Optimum current drive was found for trajectories with tangency point on the low field side.

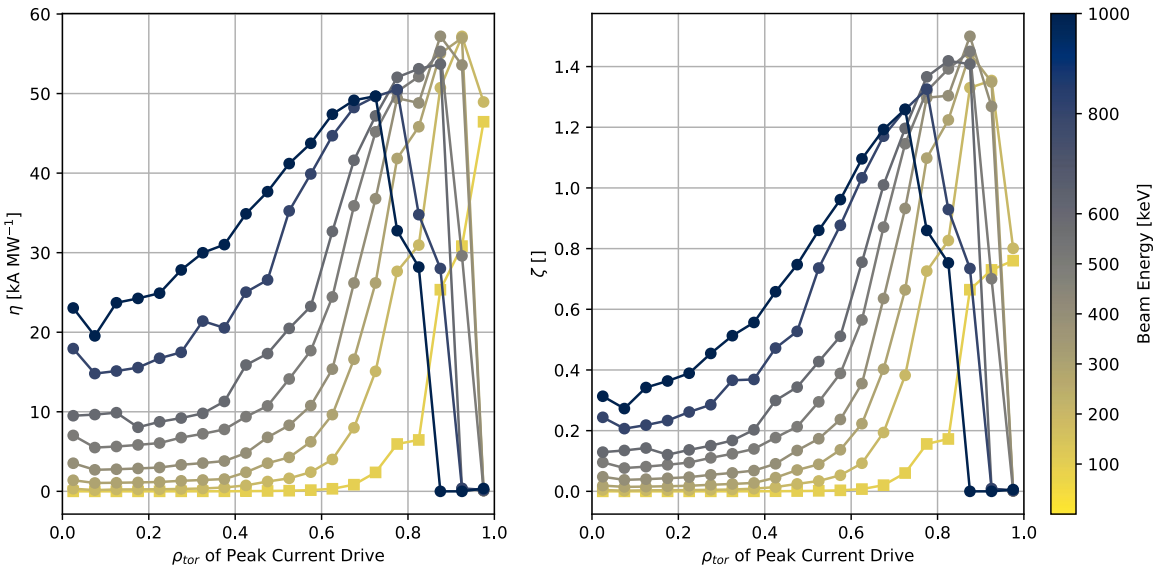

Figure 3: Maximum current drive efficiency η [kA/MW] and normalised efficiency ζ vs root normalised toroidal flux coordinate of peak in current drive profile from PENCIL. The radial location of the peak in the current profile has been binned with width $\rho_{tor} = 0.05$. *Simulations with shinethrough* $> 1\%$ *total power have been excluded.*

For each injection energy we also calculate the shinethrough as a function of the tangency radius and height. The 1% shinethrough contour is plotted in Figure 4 overlaid on the flux surface contours of the magnetic equilibrium. The shinethrough is relatively insensitive to injection energy from 100 keV to 500 keV and the beam is fully absorbed so long as the profile lies completely within the last closed flux surface. At 1000 keV the shinethrough is slightly more limiting but only restricts injection to $\rho_{tor} < 0.9$. The increase in shinethrough for tangency radii close to 0 is due to having a very normal injection trajectory, however these trajectories are not useful for current drive due to the small toroidal component of the fast ion velocity.

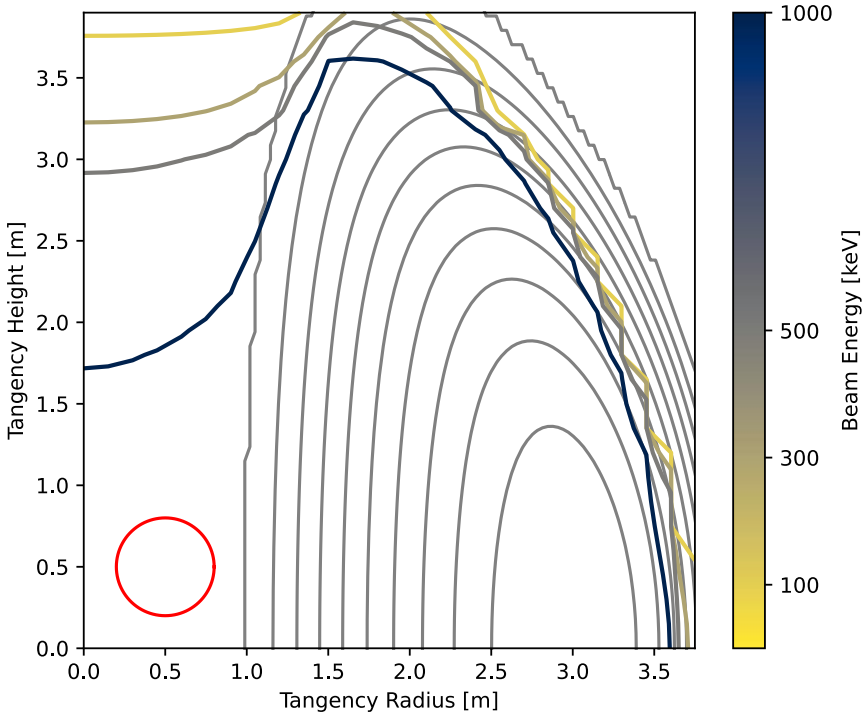

Figure 4: Contour of 1% shinethrough calculated from PENCIL as a function of the tangency radius and height for $100keV$, $300keV$, $500keV$ and $1000keV$. Contours of normalised poloidal flux for the magnetic equilibrium from 0.1 to 1 are shown in grey. For reference the size of the beam is also shown in red in the bottom left.

A scan was then performed in ASCOT based on the PENCIL scan. All tangency points on the high field side were removed. The injection energies selected were 300, 500 and 1000 keV, representing the minimum energy to penetrate the pedestal, the maximum energy possible for a JT-60SA injector and the minimum energy to penetrate to the magnetic axis respectively. The same process was applied as the PENCIL scans to generate profiles of maximum η and ζ which is shown in Figure 5.

For 300 keV, the current drive efficiency is high for $\rho_{tor} > 0.7$ but decreases rapidly moving inwards with limited efficiency inside $\rho_{tor} < 0.6$ and no penetration for $\rho_{tor} < 0.3$. Injection for $\rho_{tor} > 0.9$ is not possible due to excessive shinethrough.

The current drive efficiency increases for 500 keV, with a slight improvement over the 300 keV case as the deposition approaches mid radius. There is no penetration for $\rho_{tor} < 0.2$ so an ITER-like injector is required for on axis current drive. As for the 300 keV case, injection for $\rho_{tor} > 0.9$ is not possible due to excessive shinethrough.

The current drive further increases for 1000 keV with good efficiency achieved across the entire plasma radius. Injection for $\rho_{tor} > 0.8$ is not possible due to excessive shinethrough. The raw current drive efficiency (kA/MW) peaks near $\rho_{tor} = 0.5$, which has also been seen in DEMO studies and is suggested to be due to increased trapped electron effects off axis dominating the decrease in temperature compared to the core [29]. NBCD is generated by insufficient screening of the fast ion current by electrons so increased electron trapping is beneficial [26].

The current drive efficiencies are similar order to those for ITER [6] and DEMO [7][29], with $\zeta = 0.6 - 0.7$ given for on axis NBCD at 1MeV in ITER and DEMO and $\zeta = 0.75$ for off axis NBCD in DEMO. STEP only achieves $\zeta \sim 0.4$ but it is possible 1MeV is too low energy for peak core current drive. Note that similar discrepancies have been observed in ITER modelling between OFMC and NUBEAM likely down to different calculation of the electron shielding factor so exact agreement is not expected [6][29].

First orbit losses are found to be a less restrictive constraint than shinethrough on injection parameters. The first orbit losses are negligible then suddenly increase for injection close to the last closed flux surface, similar to what was seen in DEMO modelling [30]. Thus the shinethrough is found to be the more restrictive constraint than the first orbit loss.

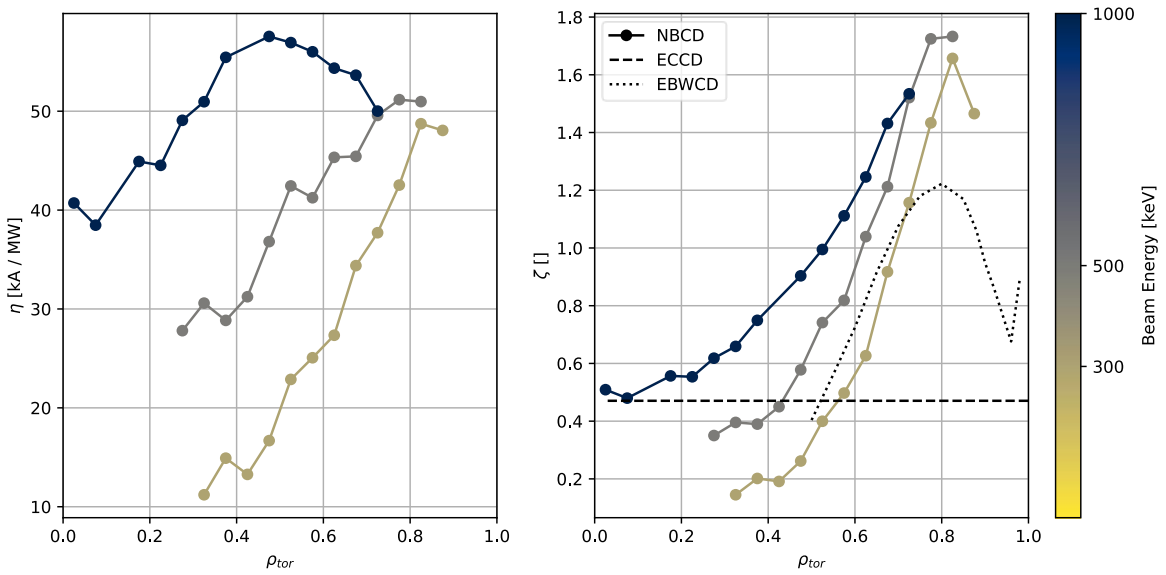

Figure 5: Maximum current drive efficiency η [kA/MW] and normalised efficiency ζ vs root normalised toroidal flux coordinate of peak in current drive profile from ASCOT. The radial location of the peak in the current profile has been binned with width $\rho_{tor} = 0.05$. Simulations with shinethrough and first orbit losses $> 1\%$ total power have been excluded. Empty bins are not marked. Equivalent ζ profiles for ECCD (dashed) and EBWCD (dotted) are also shown.

The current drive profile and tangency point overlaid on the flux surfaces of the magnetic equilibrium are plotted in Figure 6. For 500 keV and 1000 keV the current profiles are reasonably well localised about the radial location of the peak in the profiles, though the deepest penetrating 500 keV profiles develop long tails towards $\rho_{tor} = 1$. At 300 keV the profiles with peaks $\rho_{tor} < 0.5$ are very broad, hence despite the curves in Figure 5 for 300 keV and 500 keV terminating in a similar radial location in reality 300 keV would only be useful for current drive for $\rho_{tor} \geq 0.5$.

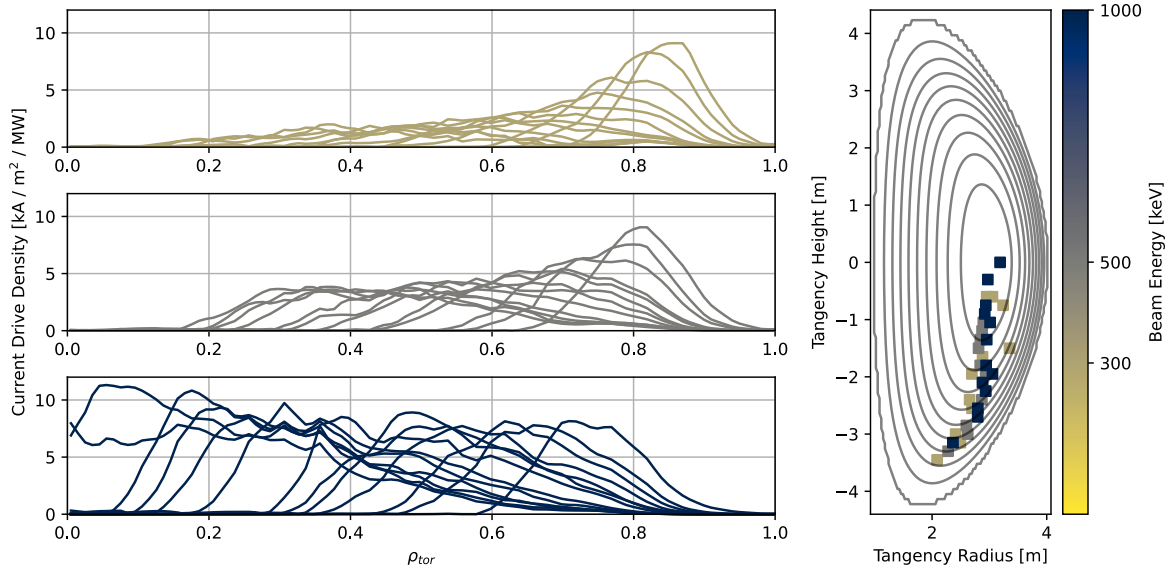

Figure 6: Current drive efficiency profiles for $300keV$ (left, top), $500keV$ (left, middle) and $1000keV$ (left, bottom), and tangency point (right) for the data points shown in Figure 4. The peak of the beam driven current profiles are localised but have long tails towards $\rho_{tor} = 1$. For $300keV$ the current drive profiles close to the core are very broad and not well localised about the peak.

The ASCOT scans also estimated the fractional power to the electron and ions, shown in Figure 7. The cases with high current drive efficiency show a high fractional power to the electrons. Equipartition of power to ions and electrons can be achieved at 300 keV, but power is dominantly transferred to electrons with increasing beam energy, as expected.

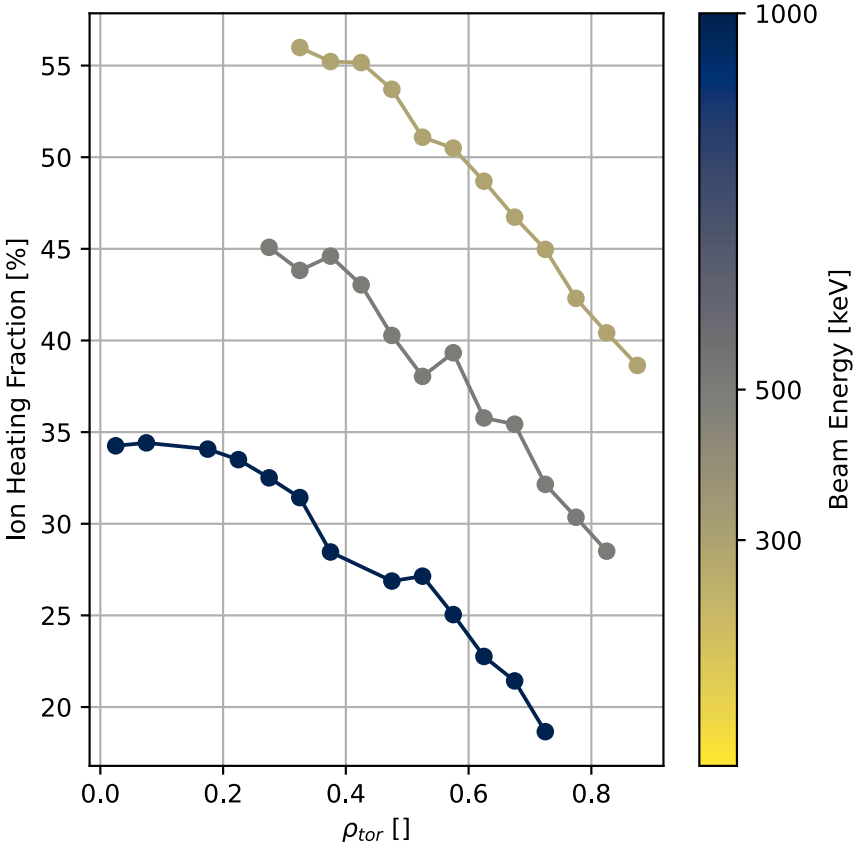

Figure 7: Ion heating fraction for the injection parameters giving optimal current drive in each radial bin as shown above. The high plasma temperature in STEP means there is still significant ion heating fraction despite the high beam energies considered.

Plasma impurities can impact the current drive efficiency. NBCD works due to an imbalance between the beam generated fast ion current and the screening electron current. This can occur due to differences in collisionality between electrons and fast / bulk ions from differing Z_{eff} or the screening electrons becoming trapped. The electron trapping is the dominant term in the screening factor for STEP as STs have a high trapped fraction [24]. This is confirmed by a scan in Z_{eff} with ASCOT which showed only a 5% change in the total driven current for a 500 keV test case when Zeff was varied from 1.5 to 3. Note the small variation is attributed to a change in deposition location rather than collisionality.

5.2 Dimensional Limitations

The ITER-like injector at 1000 keV provided the best current drive efficiency over the entire range $\rho \leq 0.8$. A beamline with dimensions of JT60-SA can fit into the lower port while the full sized ITER injector does not. This gives a maximum of 10 MW injected per port.

Given the achievable off axis current drive of 50-55 kA/MW, to generate ~ 4 MA of auxiliary current drive requires a minimum of $75 - 100$ MW installed NB power, depending on whether a 500 or 1000

keV injector is used. Adding some redundancy, a minimum of 10 ports are required to accommodate this much NBI power.

The neutral beam has a large cross section, thus the threading of the injector between the toroidal (TF) and poloidal (PF) field coils limits the achievable injection angles. Integration of a JT-60SA and ITER sized injector into the STEP CAD model indicated that injectors can be oriented between the toroidal field coils for the required toroidal steering. The arrangement of the poloidal field coils prevented any vertical tilting at the equatorial plane but some poloidal steering of the top or bottom ports towards the midplane is possible. However, such steering decreases the current drive efficiency as the beam trajectory becomes more normal to the poloidal magnetic field, effectively limiting $\beta = 0$.

An up down asymmetry in NBCD has been observed on MAST [10], which is a much stronger effect in STs compared to conventional aspect ratio due to the steep magnetic pitch angle. This is also observed in ASCOT simulations. For example, repeating the optimal injection for $\rho = 0.5$ (300 keV, $R_T = -2.9$m, $Z_T = 2.6$m) mirrored across the midplane ($Z_T = -2.6$m) only generated 25% of the current. To avoid this degradation in STEP injection is restricted to the equatorial or lower port.

The neutron flux is maximal at the equatorial plane and decreases towards the upper and lower. Penetrations at the equatorial plane therefore result in maximum reduction in tritium breeding. STEP is intended also to demonstrate tritium self-sufficiency and therefore targets a tritium breeding ratio (TBR) > 1.1. MCNP modelling estimated the ten injectors would reduce the TBR by 0.25 when only using the equatorial ports.

This is an enormous reduction and is also likely an under-estimate as the calculation only considered the spatial loss, neglecting the effect of absorption by the shielding materials that would be required to surround the port. To ensure TBR > 1.1, the NB injectors are thus further confined to only the lower ports. This severely constrains the access to $\rho > 0.7$ as the poloidal field coils prevent the poloidal steering required to recover line of sight to the plasma core.

5.3 Ramp Up / Down

NBI operation in the ramp up is limited by the shinethrough. The kinetic profiles in the ramp up are approximated by scaling the n_e profile to $10 - 50\%$ of the flat top value in 5% steps. The T_e profile is not changed. At each density scaling, a scan is performed to evaluate shinethrough varying injection energy E_b from 100 to 1000 keV in 100 keV steps, source height Z_s from 0 to 4m in 0.15m steps and tangency radius R_T from 1.5 to 4m in 0.15m steps. The source radius R_s was set at 6m and the tangency height Z_T was set equal to Z_s. This scan is ideally suited for PENCIL, which has accurate absorption and hence shinethrough calculation and can rapidly scan though a large parameter space.

For each injection energy and tangency point, the shinethrough at each density scaling was used to determine the minimum volume averaged density with shinethrough $< 1\%$ total power. Each scan point was then binned by ρ_{tor} of the peak in the current driven profile using the same procedure as the flat top scans. The minimum volume averaged density at the bin centres was then taken as the threshold density required for NB deposition as a function of ρ_{tor}.

The results of this process are illustrated in Figure 8, with the position of the maximum in current drive density on the x-axis and minimum acceptable density on the y-axis. The second y-axis shows the equivalent current corresponding to setting the volume averaged density to the Greenwald density.

The shinethrough limits are far more restrictive than that predicted for ITER [6] or DEMO [30] but is not surprising as shinethrough increases with acceleration energy and decreases for larger integrated density along the beam trajectory, the latter of which is reduced in a ST due to the smaller minor

radius. However, very high current drive efficiency can be expected in the ramp-up as the efficiency broadly scales like T_e/n_e.

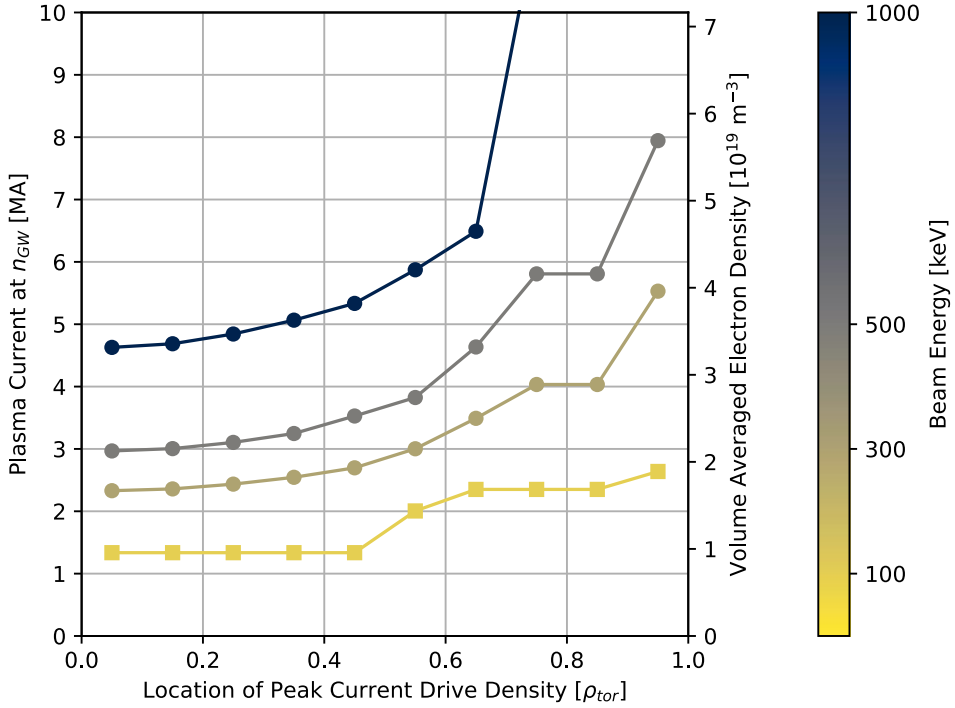

Figure 8: Minimum volume averaged density [$10^{19} m^{-3}$] and the corresponding minimum plasma current [MA] at the Greenwald limit where shinethrough < 1% injected power. The x position shows where the normalised toroidal flux coordinate of the maxima in the beam driven current profile.

The plasma current is expected to be $1-2$ MA at the end of the breakdown and burn-through [2]. This is set by the size of the solenoid that can fit into the centre column. A minimum of 1.5MA of plasma current is required at 100 keV, around 3MA for 300 keV and almost 7MA for 1 MeV. This is a lower bound as the ramp up will almost certainly take place at Greenwald fractions $< 100\%$. It would be a major challenge to accommodate a solenoid capable of ramping the plasma current high enough to operate at the beam energies considered for flat top (≥ 300 keV).

The NBI system will be optimised for beam size at the highest energy operation. The beam optics will be optimised for high power operations, so at fixed perveance the beam power $P \propto E_b^{2.5}$ [12] thus operating even a 300 keV beam at 100 keV would only generate 6.4% of the power. The required HCD power in the ramp will scale linearly with I_p but the available NBI power scales like a power law while I_p is less than the shinethough defined minimum. Thus there will not be enough NBI power available to ramp to the shinethough defined minimum current.

Therefore, the only possibility would be to install a lower energy beam system dedicated for low density phases. However, given the challenges of integrating a single NBI system into the tokamak complex, integrating two is not realistic.

It is therefore clear NBI cannot solely provide the non-inductive current drive required during the ramp-up and ramp-down phases as there is no overlap between the achievable plasma current at the end of the inductive phase of the ramp and the minimum plasma current required for acceptable shinethrough. An additional HCD system would be therefore required to assist in the initial ramp-up and final ramp-down phases.

6 Engineering Relevant Issues

As STEP is to generate net electrical power and the HCD system is the largest component of the parasitic load, to determine the optimum STEP HCD mix highest priority was placed on driving bulk plasma current in the flat top as efficiently as possible. A low grid-to-plasma efficiency η_{HCD} therefore negates the advantages of efficient current drive in plasma, at least at $Q \sim 11$ targeted for STEP.

STEP initially targeted $\eta_{HCD} \geq 0.42$ whereas present NBI technology has $\eta_{HCD} \approx 0.26$ [31]. This can theoretically be increased by development of plasma-based neutralisers or active recovery of the residual ions [31]. An ITER-like injector for DEMO with a plasma neutraliser has a predicted $\eta_{HCD} \approx 0.39$ [31], falling short of the STEP target. Furthermore, such technology is not available and requires major R&D to develop. Concepts for photo-neutralisers could further improve the efficiency but such technology is not going to be available either on DEMO or STEP timelines [32]. However, even if all the proposed R&D to improve wall plug efficiency were realised it would still be low compared to radio wave and microwave frequency based HCD systems.

No existing NBI system has demonstrated injection at energies > 500 keV into a tokamak. An R&D programme to develop 1MeV negative ion injectors is ongoing as part of ITER though it is uncertain when such a system would available.

Another concern for the NBI system is integration around the tokamak. A negative ion beam injector tends to have a size comparable to the tokamak itself. Arranging ten injectors inside the nuclear island greatly increases its size and the size of the larger tokamak building complex and is a nearly unsurmountable integration challenge. Having large numbers of components inside the nuclear island represents a significant maintenance and inspection challenge. This also runs contrary to the motivation of using a ST in the first place, to minimise the device and building size to reduce costs.

After the conclusion of this analysis, it was decided the STEP machine would increase in size. While this appears beneficial for some of the issues discussed above, it does not change the conclusions. The equatorial ports remain unavailable for NB in a ST reactor as the degradation of the TBR is too severe. A larger machine necessitates higher acceleration energies, effectively demanding $E_b > 500$ keV which are even more technologically immature. This also negatively impacts core current drive as E_b cannot exceed $1\ \mathrm{MeV}$ thus the achievable core NBCD efficiency would decrease. The fundamental issues of low wall-plug efficiency and lack of availability outside the flat top and for core current drive also persist.

7 Complete Assessment

This study has shown NBCD in STEP to be highly efficient, achieving efficiencies only exceeded by Electron Bernstein Waves (EBW) for deposition $\rho \leq 0.8$ [33]. Theoretically, a NBI system on STEP could deliver ~ 4MA of current from 100MW injected at 1MeV and 130MW injected at 500 keV, with a 30% redundancy. However, such an NBI system has significant limitations:

1. Only off-axis current drive $\rho \geq 0.7$ is achievable, as only lower ports can be used to maintain a tritium breeding ratio > 1.1.
2. An additional HCD system is required for on axis current drive in the flat top for complete control of the current profile.
3. An additional HCD system is required for plasma start-up, ramp-up and ramp-down.
4. The optimum current drive efficiency requires injection energies $\geq 500\ keV$ for which there are no existing systems.
5. The plug to plasma electrical efficiency $\eta_{HCD} \approx 0.26$ is much lower than the requirement $\eta_{HCD} = 0.42$ estimated for STEP to generate net electrical power.

6. An NBI system would significantly increase the size and cost of the tokamak complex, negating much of the cost savings associated with a compact spherical tokamak.

Considering the above, the recommendation for the optimum STEP HCD mix was to not consider NBI. The decision was to proceed with a fully microwave based system utilising the strengths of both the electron cyclotron and Electron Bernstein Wave to achieve STEP's HCD functional requirements [34].

8 Acknowledgements

The authors would like to thank the support of Emmi Tholerus (ASCOT), Florian Koechl (JETTO/JINTRAC), Damian King (PENCIL) and James Hague (TBR Modelling).

9 References

[1] I. T. Chapman and A. W. Morris, "UKAEA capabilities to address the challenges on the path to delivering fusion power," *Philosophical Transactions of the Royal Society A*, vol. 377, no. 2141, p. 20170436, 2019.

[2] E. Tholerus *et al.*, "Flat-top plasma operational space of the STEP power plant," *Nuclear Fusion*, 2024, Accessed: Sep. 11, 2024. [Online]. Available: https://iopscience.iop.org/article/10.1088/1741-4326/ad6ea2/meta

[3] M. C. R. de Andrade and G. O. Ludwig, "Scaling of bootstrap current on equilibrium and plasma profile parameters in tokamak plasmas," *Plasma Phys Control Fusion*, vol. 50, no. 6, p. 65001, 2008.

[4] C. D. Challis *et al.*, "Non-inductively driven currents in JET," *Nuclear Fusion*, vol. 29, no. 4, p. 563, 1989.

[5] E. Hirvijoki *et al.*, "ASCOT: Solving the kinetic equation of minority particle species in tokamak plasmas," *Comput Phys Commun*, vol. 185, no. 4, pp. 1310–1321, 2014.

[6] F. Wagner *et al.*, "On the heating mix of ITER," *Plasma Phys Control Fusion*, vol. 52, no. 12, p. 124044, 2010.

[7] G. Giruzzi *et al.*, "Modelling of pulsed and steady-state DEMO scenarios," *Nuclear Fusion*, vol. 55, no. 7, p. 73002, 2015.

[8] T. H. Stix, "Heating of toroidal plasmas by neutral injection," *Plasma Physics*, vol. 14, no. 4, p. 367, 1972.

[9] B. Geiger *et al.*, "Fast-ion transport and neutral beam current drive in ASDEX upgrade," *Nuclear Fusion*, vol. 55, no. 8, p. 83001, 2015.

[10] M. Turnyanskiy *et al.*, "Study of the fast ion confinement and current profile control on MAST," *Nuclear Fusion*, vol. 49, no. 6, p. 65002, 2009.

[11] M. Giacomin *et al.*, "On electromagnetic turbulence and transport in STEP," *Plasma Phys Control Fusion*, vol. 66, no. 5, p. 55010, 2024, Accessed: Sep. 11, 2024. [Online]. Available: https://iopscience.iop.org/article/10.1088/1361-6587/ad366f/meta

[12] D. Ćirić *et al.*, "Performance of upgraded JET neutral beam injectors," *Fusion Engineering and Design*, vol. 86, no. 6–8, pp. 509–512, 2011.

[13] A. Kojima *et al.*, “Achievement of 500 keV negative ion beam acceleration on JT-60U negative-ion-based neutral beam injector,” *Nuclear Fusion*, vol. 51, no. 8, p. 83049, 2011.

[14] Y. Takeiri *et al.*, “High performance of neutral beam injectors for extension of LHD operational regime,” *Fusion Science and Technology*, vol. 58, no. 1, pp. 482–488, 2010.

[15] R. S. Hemsworth *et al.*, “Overview of the design of the ITER heating neutral beam injectors,” *New J Phys*, vol. 19, no. 2, p. 25005, 2017.

[16] I. Jenkins, C. D. Challis, D. L. Keeling, and E. Surrey, “Scoping studies for NBI launch geometries on DEMO,” *Fusion Engineering and Design*, vol. 106, pp. 9–16, 2016.

[17] M. Romanelli *et al.*, “JINTRAC: a system of codes for integrated simulation of tokamak scenarios,” *Plasma and Fusion research*, vol. 9, p. 3403023, 2014.

[18] M. Kovari, R. Kemp, H. Lux, P. Knight, J. Morris, and D. J. Ward, “‘PROCESS’: A systems code for fusion power plants—Part 1: Physics,” *Fusion Engineering and Design*, vol. 89, no. 12, pp. 3054–3069, 2014.

[19] R. L. Miller, M.-S. Chu, J. M. Greene, Y. R. Lin-Liu, and R. E. Waltz, “Noncircular, finite aspect ratio, local equilibrium model,” *Phys Plasmas*, vol. 5, no. 4, pp. 973–978, 1998.

[20] E. Tholerus *et al.*, “Flat-top plasma operational space of the STEP power plant,” *arXiv preprint arXiv:2403.09460*, 2024.

[21] H. P. Summers, “The ADAS user manual, version 2.6,” *http://www. adas. ac. uk/*, 2004.

[22] O. Asunta *et al.*, “Modelling neutral beams in fusion devices: Beamlet-based model for fast particle simulations,” *Comput Phys Commun*, vol. 188, pp. 33–46, 2015.

[23] D. R. Mikkelsen and C. E. Singer, “Optimization of steady-state beam-driven tokamak reactors,” *Nuclear Technology-Fusion*, vol. 4, no. 2P1, pp. 237–252, 1983.

[24] D. F. H. Start and J. G. Cordey, “Beam-induced currents in toroidal plasmas of arbitrary aspect ratio,” *Phys Fluids*, vol. 23, no. 7, pp. 1477–1478, 1980, doi: https://doi.org/10.1063/1.863134.

[25] T. C. Luce *et al.*, “Generation of localized noninductive current by electron cyclotron waves on the diii-d tokamak,” *Phys Rev Lett*, vol. 83, no. 22, p. 4550, 1999.

[26] N. J. Fisch, “Theory of current drive in plasmas,” *Rev Mod Phys*, vol. 59, no. 1, p. 175, 1987, Accessed: Sep. 11, 2024. [Online]. Available: https://journals.aps.org/rmp/abstract/10.1103/RevModPhys.59.175

[27] P. Vincenzi *et al.*, “Optimization-oriented modelling of neutral beam injection for EU pulsed DEMO,” *Plasma Phys Control Fusion*, vol. 63, no. 6, p. 65014, 2021.

[28] M. Kuriyama *et al.*, “Operation and development of the 500-keV negative-ion-based neutral beam injection system for JT-60U,” *Fusion science and technology*, vol. 42, no. 2–3, pp. 410–423, 2002.

[29] H. Zohm *et al.*, “Assessment of H&CD system capabilities for DEMÓ,” in *40th EPS Conference on Plasma Physics*, 2013.

[30] P. Vincenzi, J.-F. Artaud, E. Fable, G. Giruzzi, M. Siccinio, and H. Zohm, “Neutral beam injection for DEMO alternative scenarios,” *Fusion Engineering and Design*, vol. 163, p. 112119, 2021.

[31] M. Q. Tran *et al.*, “Status and future development of heating and current drive for the EU DEMO,” *Fusion Engineering and Design*, vol. 180, p. 113159, 2022.

[32] R. McAdams, “Beyond ITER: Neutral beams for a demonstration fusion reactor (DEMO),” *Review Of Scientific Instruments*, vol. 85, no. 2, 2014.

[33] T. Wilson *et al.*, “Electron Bernstein Wave (EBW) current drive profiles and efficiency for STEP,” in *EPJ Web of Conferences*, 2023, p. 1011.

[34] S. Freethy *et al.*, “Microwave current drive for STEP and MAST Upgrade,” in *EPJ Web of Conferences*, 2023, p. 4001.